Record-Breaking Precipitation in Indonesia's Capital Jakarta in January 2020 Linked to the Northerly Surge, Equatorial Waves, and MJO

Sandro W. Lubis[1,1], Samson Hagos[1,1], Eddy Hermawan[2,2], Muhamad Reyhan Respati[3,3], Ainur Ridho[4,4], Fadhlil R. Muhammad[5,5], Jaka A. I. Paski[6,6], Dian Nur Ratri[6,6], Sonny Setiawan[7,7], Donaldi S. Permana[8,8], Risyanto Risyanto[2], and Siswanto Siswanto[9]

[1]Pacific Northwest National Laboratory (DOE)
[2]National Research and Innovation Agency
[3]School of Earth, Atmosphere and Environment, Monash University
[4]Search Engine for Risk and Actions on Resilience
[5]School of Earth Sciences, University of Melbourne
[6]Indonesia Agency for Meteorology Climatology and Geophysics
[7]Department of Geophysics and Meteorology, IPB University
[8]Indonesian Agency for Meteorology Climatology and Geophysics
[9]Indonesia Meteorological, Climatological, and Geophysical Agency

November 30, 2022

Abstract

A rare record-breaking extreme rainfall event, the highest amount recorded since 1866, hit Indonesia's capital, Jakarta, in early January 2020. The torrential rainfall was mainly caused by an active cross-equatorial northerly surge (CENS) that occurred concurrently with equatorial waves and Madden-Julian oscillation (MJO). A strong and persistent low-level northerly wind and moisture transport induced by CENS created favorable atmospheric conditions for the formation of deep convection and heavy rainfall over Jakarta. The concurrent occurrences of convectively active phases of equatorial waves (mainly Kelvin, TD-type, and eastward propagating inertia-gravity waves) and MJO during the event further supported the development of heavy rainfall by increasing low-level moisture flux convergence, whereas equatorial Rossby waves contributed indirectly to the increased moisture transport by amplifying cross-equatorial meridional flows toward Jakarta. Together, these large-scale dynamical forcing factors provided a conducive convective environment for the development of mesoscale convective systems and, hence, extreme rainfall over the region.

Record-Breaking Precipitation in Indonesia's Capital Jakarta in January 2020 Linked to the Northerly Surge, Equatorial Waves, and MJO

Sandro W. Lubis[1*], Samson Hagos [1], Eddy Hermawan [2], Muhamad R. Respati [3], Ainur Ridho [4], Risyanto [2], Fadhlil R. Muhammad [5], Jaka A. I. Paski [6], Siswanto [6], Dian Nur Ratri [6,7], Sonny Setiawan [8], Donaldi S. Permana [6]

[1]Pacific Northwest National Laboratory, Richland, Washington, USA
[2]National Research and Innovation Agency (BRIN), Indonesia
[3]School of Earth, Atmosphere and Environment, Monash University, Australia
[4]Search Engine for Risk and Actions on Resilience, Indonesia
[5]School of Earth Sciences, University of Melbourne, Australia
[6]Indonesia Agency for Meteorology Climatology and Geophysics, Indonesia
[7]Wageningen University and Research, Netherlands
[8]Department of Geophysics and Meteorology, IPB University, Indonesia

Key Points:

- An exceptionally high daily rainfall accumulation of up to 377 mm caused severe flash floods in Jakarta in early January 2020.
- The extreme rainfall was mainly caused by the cross-equatorial northerly surge that occurred concurrently with equatorial waves and MJO.
- Equatorial waves and MJO contribute up to ∼23% to the enhanced daily precipitation during the event.

[*]902 Battelle Blvd, Richland, WA 99354, USA

Corresponding author: Sandro W. Lubis, sandro.lubis@pnnl.gov

Abstract

A rare record-breaking extreme rainfall event, the highest amount recorded since 1866, hit Indonesias capital, Jakarta, in early January 2020. The torrential rainfall was mainly caused by an active cross-equatorial northerly surge (CENS) that occurred concurrently with equatorial waves and Madden–Julian oscillation (MJO). A strong and persistent low-level northerly wind and moisture transport induced by CENS created favorable atmospheric conditions for the formation of deep convection and heavy rainfall over Jakarta. The concurrent occurrences of convectively active phases of equatorial waves (mainly Kelvin, TD-type, and eastward propagating inertia-gravity waves) and MJO during the event further supported the development of heavy rainfall by increasing low-level moisture flux convergence, whereas equatorial Rossby waves contributed indirectly to the increased moisture transport by amplifying cross-equatorial meridional flows toward Jakarta. Together, these large-scale dynamical forcing factors provided a conducive convective environment for the development of mesoscale convective systems and, hence, extreme rainfall over the region.

Plain Language Summary

A record-breaking heavy rainfall event, the highest in the 155-year historical records, hit Indonesia's capital, Jakarta, in early January 2020. The flooding induced by extreme rainfall caused tremendous damage to infrastructure and had significant socioeconomic impacts. This study examines the atmospheric driving mechanisms of this extreme event. We found that strong and persistent low-level winds of the CENS transported moisture toward Jakarta, created favorable conditions for the development of deep convection and heavy rain over the region. The large-scale moisture convergence induced by some types of equatorial waves and MJO further enhanced local moisture and supported the development of convective cells and extreme rainfall. Deepening the understanding of the atmospheric mechanisms driving this event may provide valuable information for forecasting precipitation extremes over Jakarta in the future.

1 Introduction

Jakarta, the capital megacity of Indonesia located in the northwest of Java Island, Indonesia (Fig. 1a), experienced an extraordinary heavy rainfall event in early January 2020. The highest amount reached up to 377 mm (14.83 inches) per day, making it a record-breaking number in observations since 1866. This extreme rainfall subsequently triggered widespread disastrous flooding in Jakarta and its surroundings in the early morning of 1 January 2020, leading to catastrophic losses. It is estimated that at least 173,000 people were evacuated, 66 people died, more than 60% of the residential areas were submerged, and the economic loss reached over US$700 million (Berlinger & Yee, 2020; Nisa, 2020). Because of the high vulnerability of Jakarta to rainfall extremes, a better understanding of the physical processes of heavy rainfall is needed to establish a reliable extended-range flood forecast system for this region.

Numerous studies have examined the effects of large-scale atmospheric circulation on precipitation extremes and major floods in Jakarta. For example, the major flooding event in February 2007 (the second highest record-breaking precipitation event) was attributed to an intense and persistent cross-equatorial northerly surge (CENS) that created an intensive low-level wind convergence and favorable dynamic conditions for the development of convective cells over the region (Wu et al., 2007; Trilaksono et al., 2011; Hattori et al., 2011). Other studies also showed the potential role of Madden Julian oscillation (MJO) in driving extreme rainfall and major floods in Jakarta (Wu et al., 2007; Aldrian, 2008; Wu et al., 2013; Nuryanto et al., 2019). In particular, Wu et al. (2013) reported that the extreme precipitation that caused a major flooding event in January

2013 was associated with the strong low-level convergence of winds induced by the active phase of the MJO. The enhanced convection induced by MJO contributed to the growth of the mesoscale convective system (MCS) and brought heavy rainfall from its activity over the region (Nuryanto et al., 2019, 2021). Other major Jakarta flooding events in February 2002, 2008, and 2015, were also linked to similar causes, with unusual northerly winds associated with a CENS and the convective phases of MJO (Wu et al., 2007; Aldrian, 2008; Siswanto et al., 2015).

Notwithstanding the importance of CENS and MJO in extreme rainfall events, recent studies have found that equatorially trapped waves, including Kelvin waves, equatorial Rossby waves, tropical-depression (TD)-type waves, eastward propagating inertio-gravity (EIG) waves, and mixed Rossby-Gravity (MRG) waves, also play a major role in organizing tropical convection and triggering torrential rains and floods (Lubis & Jacobi, 2015; Baranowski et al., 2020; Ferrett et al., 2020; Sakaeda et al., 2020; Lubis & Respati, 2021; Latos et al., 2021; Peatman et al., 2021). In general, equatorial waves organize circulation that favors either active or suppressed convection (e.g., Wheeler and Kiladis (1999); Kiladis et al. (2009)), consequently influencing the frequency and intensity of precipitation events. Lubis and Respati (2021), for example, showed that the convectively active phases of Kelvin waves increased the probability of extreme rains over Java by about 30%-60%. Baranowski et al. (2020) also found evidence that Kelvin waves play a critical role in the majority of flooding events in Sumatra. Similarly, Latos et al. (2021) reported that Kelvin waves and equatorial Rossby waves can double the probability of floods and extreme rain events in Sulawesi. Despite clear evidence from these regional studies, it remains elusive whether equatorial waves contributed to the major flooding incident in Jakarta in early January 2020.

This study investigates the atmospheric driving mechanisms of the exceptionally extreme rainfall and devastating floods in Jakarta in early January 2020. We focus on the role of large-scale meteorological drivers in modulating large-scale circulations and moisture transport that favor the development of deep convection and local, extreme precipitation event in Jakarta using in situ measurements, satellite data, meteorological radar observations, and reanalysis data. The current study provides a complete picture of the large-scale meteorological drivers of the major flood in Jakarta in early January 2020.

2 Data

2.1 Satellite Data

The Integrated Multi-satellite Retrievals (IMERG) data from NASA (Huffman et al., 2020) are used for the period of 1 January 2001 to 30 December 2020, with an hourly temporal resolution and on a $0.1^\circ \times 0.1^\circ$ grid. Recent studies have shown that satellite-based precipitation data like IMERG have good capability to observe rainfall variability over the Maritime Continent (Ramadhan et al., 2022) and detect extreme events with short return-periods such as those affected by equatorial waves and MJO (Lubis & Respati, 2021; Schreck, 2021). We also use the Himawari-8 satellite image of IR13 (infrared channel 13) (Bessho et al., 2016) with a spatial resolution of 4 km and a temporal resolution of an hour to observe the development of large mesoscale convective clouds (see Section 3.1).

2.2 C-band Doppler Radar Data

The Gematronik C-band Doppler radar located in Soekarno-Hatta meteorological station (106.6502°E, 6.1669°S, 30 m above mean sea level, with maximum radius coverage of 250 km) is used to derive the high resolution local rainfall field for a period of 31 December 2019 - 1 January 2020. The three-dimensional reflectivity and Doppler velocities are recorded every 8 minutes in a volumetric format consisting of nine plan in-

dicator scans from 0.5° to 19.5° with reflectivity values in decibels (dBZ). Radar data is processed using *wradlib* Python library developed by Heistermann et al. (2013). The ground clutter caused by non-meteorological factors (e.g., mountains, hills, tall buildings) and objects in the air (e.g., aircraft, birds, etc.) are removed by using a texture-based technique developed by Gabella and Notarpietro (2002). We also apply an attenuation correction algorithm to remove random radar noises (Krämer & Verworn, 2009). The reflectivity data is gridded and displayed as Column Maximum (CMAX) and conversion of reflectivity (dBz) into rainfall intensity (mm/hr) follows the method used by BMKG (e.g., Paski et al. (2020)). In this method, the quantitative precipitation estimation (QPE) value is derived from a common Z-R relationship of Marshall et al. (1947) with $Z = AR^b$, where A =200R, b=1.6, Z is the reflectivity factor, and R is the rainfall rate.

2.3 In Situ Data, Renalysis, and Other Data

We use hourly and daily rainfall measurements from 5 stations located around Jakarta (namely Kemayoran, Halim Perdana Kusumah, Cengkareng, Tanjung Priok, and Pondok Betung) for the period of December 31, 2019 - January 1, 2020 operated by the Agency for Meteorology, Climatology and Geophysics of the Republic of Indonesia (BMKG).

Meteorological fields from the fifth generation European Centre for Medium-Range Weather Forecasts (ECMWF ERA5) reanalysis (Hersbach et al., 2020) from January 1, 1980 - December 31, 2020 on a regular 0.25° grid with an hourly temporal resolution are used to evaluate large-scale synoptic conditions and to analyze moisture transport and wave analysis during the event. We also uses gridded daily outgoing longwave radiation (OLR) data from National Oceanic and Atmospheric Administration (NOAA) on a 2.5° × 2.5° grid for the period of 1 January 1979 to 31 December 2020 (Liebmann & Smith, 1996) and NOAA Optimum Interpolation (OI) Sea Surface Temperature (SST) V2 data (Reynolds et al., 2002). SST anomalies are calculated relative to 1971-2000 climatology.

3 Methods

3.1 Tracking of mesoscale convective system (MCS)

A graph theory based algorithm (GTG) (Whitehall et al., 2015) is used for automated identification and characterization of a large mesoscale convective system (MCS). The GTG algorithm can handle the complex evolution of the MCS, as it allows MCS to have multiple cloud element (CE) simultaneously at one time frame. Tracking of MCS is performed by applying the GTG algorithm to the hourly brightness temperature (TBB) data from the Himawari-8 satellite. In this study, MCS as a convective system is defined as contiguous pixels with TBB $<$ 243 K and with an area $\geq$ 2400 km^2 or a smaller area where there exists a convective core such there is at least 10 K brightness temperature range. These criteria must be fulfilled and last continuously for longer than 3 hr (see the detailed procedures in Whitehall et al. (2015)). Application of the GTG algorithm for detection of MCSs over the Maritime Continent has been found to be reliable as multiple merging of convective cells frequently occurs over the region (Nuryanto et al., 2019, 2021).

3.2 HYSPLIT Model and Backward Trajectories

The mechanisms of moisture transport and the origins of extreme precipitation over Jakarta in early January 2020 are still uncertain. In this study we employ a backward trajectory analysis to track the moisture source using a Hybrid Single-Particle Lagrangian Integrated Trajectory (HYSPLIT) model version 5.1 (Stein et al., 2015). We run the model every 3 hr starting at 2100 UTC on 31 December 2019 (i.e., the highest peak of precipitation event) to generate 72-hr backward trajectories (from 500 to 2,000 m) above the

ground in the 50 target points around Jakarta with a horizontal interval of 0.25° deg (see Fig. 2(k)). We chose this altitude range because water vapor is highly concentrated in the lower troposphere. In addition, we also calculate relative moisture source contributions using a similar algorithm proposed by Nie and Sun (2022) (see Text S1 and Fig. S1 in Supporting Information for ~~a~~ detailed information). The three-dimensional meteorological variables, such as specific humidity, winds, and geopotential height used in the model are obtained from ERA5 reanalysis (Hersbach et al., 2020).

3.3 Filtering technique and wave analysis

To isolate the equatorial wave signals in precipitation and other dynamical fields, we employ a two-dimensional fast Fourier transformation (2D FFT) filtering technique (Wheeler & Kiladis, 1999; Kiladis et al., 2009). The wavenumber-frequency domains of each wave mode used in the filtering technique are similar to Kiladis et al. (2009) and Lubis and Jacobi (2015) (Table S1 in Supporting Information). Furthermore, to retrieve the local phases and amplitudes of equatorial waves, we use a similar approach proposed by Riley et al. (2011) (see Text S2 in Supporting Information). The constructed local phase diagrams (shown later in Figs. 3b-g) reveal~~s~~ the time-evolution of wave activity above Jakarta with a reference longitude of 106.5°E. Cool colors (phases 4-6) indicate enhanced regional convection by the equatorial wave, whereas warm colors (phases 8, 1-2) correspond to suppressed regional convection.

3.4 Water vapor transport and moisture flux convergence

To understand the underlying mechanisms of equatorial wave and MJO modulation on extreme rainfall, we also calculate vertically integrated water vapor transport (IVT) and vertically integrated moisture flux convergence (VIMFC) associated with different types of equatorial waves and MJO. The IVT and VIMFC are calculated from total fields and then filtered with respect to the different frequency-wavenumber domains (Table S1 in Supporting Information). The IVT is calculated using ERA5 zonal and meridional winds and specific humidity (see Text S3 in Supporting Information for more details).

4 Characteristics of Heavy Rainfall

Figure 1 shows the characteristics of precipitation during the period from 31 December 2019 to 1 January 2020, over the flood zone. During this period, heavy rainfall covered most areas in Jakarta, with higher intensity in the eastern part of the city (Fig. 1a). Based on the averaged in situ data from five stations, the first peak reached 20±14 mm/hour at 1000 UTC on 31 December, and the second peak of rainfall reached 39±28 mm/hour at 2100 UTC on 1 January (Fig. 1b). These results were confirmed by radar and satellite observations, though there were differences in the amplitude and timing of precipitation (Figs. 1b-c). In particular, the radar estimates were low compared to the in situ and satellite observations, possibly due to bias in calibration, correction, and QPE (e.g., Paski et al. (2020)).

Daily rainfall measurements from five meteorological stations in Jakarta indicated that the highest rainfall accumulation of up to 377 mm per day was recorded at Halim Perdana Kusumah (PK) Air Force Base in East Jakarta (Fig. 1d). This event was unprecedented in Jakartas historical rainfall database since 1866 (Fig. S2 in Supporting Information) and is estimated to have a return period of 300 years (Fig. 1e). This return period is much longer than the previous major flood event reported in 2015, which is expected to occur once every 139 years (Siswanto et al., 2015). It is also clear from the time series of the highest annual rainfall events that changes in the intensity of maximum daily rainfall in Jakarta have tended to increase by 15.41 mm/decade (Fig. 1d and Fig. S2 in Supporting Information).

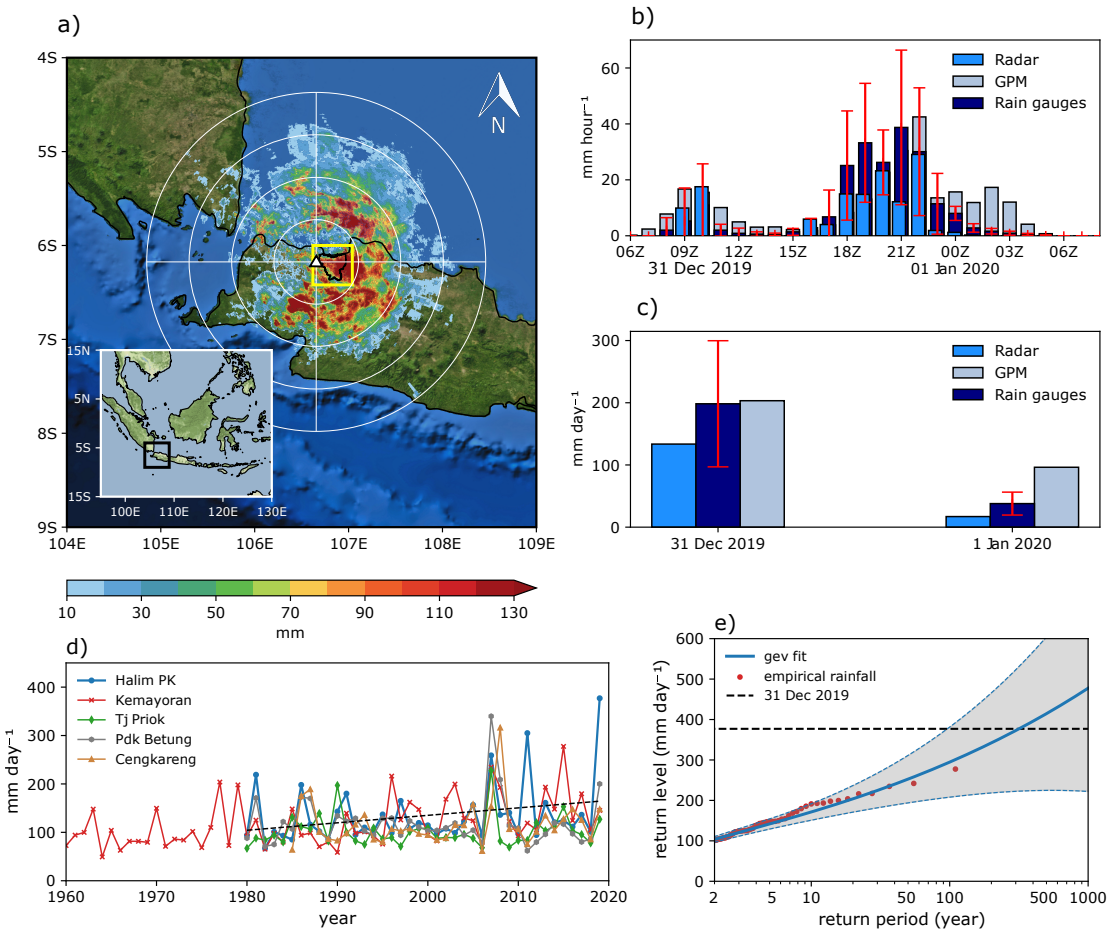

Figure 1. (a) Total precipitation (mm) estimated by C-band Doppler radar located in Soekarno-Hatta meteorological station from 31 December 2019 to 1 January 2020. Location of the city of Jakarta is qualitatively depicted by a yellow box, covering 6.00°- 6.42°S, 106.62°-107.04°E. (b) Mean hourly accumulated precipitation from GPM satellite, C-band Doppler radar averaged over the box and 5 rain gauge stations. Time is in UTC. (c) Daily mean accumulated precipitation based on GPM satellite, radar, and 5 rain gauge stations. Vertical bars in (b) and (c) denote a standard deviation of the rainfall variation among the stations. (d) Time series of annual maximum daily precipitation (RX1 day) from 5 rain gauge stations from 1960-2019 (see Fig. S1 for the longer records back to 1866). The trend line is calculated for the Halim PK rain gauge station. (e) Return period of Jakarta RX1day for the period of 1960-2019. Blue lines correspond to the GEV fit parameters for 2019 with a 95% confidence interval estimated with a non-parametric bootstrap following Siswanto et al. (2015).

5 Large-Scale Atmospheric Drivers of Heavy Rainfall

In this section, we exploit the potential attribution of large-scale meteorological phenomena to the early January 2020 extreme rain and flooding event in Jakarta. Given the fact that during this period, the Indian Ocean Dipole was in a positive phase and the El Niño-Southern Oscillation (ENSO) was in transition to its neutral phase (not shown), other large-scale phenomena beyond the low-frequency variability must have been responsible for driving the extreme event, as we discuss below.

5.1 Occurrence of a cross-equatorial northerly surge (CENS)

Strong and persistent northeasterly winds during the northeast monsoon season played a crucial role in driving the extreme rainfall event in Jakarta in early January 2020 (Fig. 2 and Fig. S3). It is evident that the northeasterly winds over the South China Sea became stronger a few days prior to the episode of heavy rainfall and were classified as an active cold surge (CS) event at 0000 UTC on 31 December 2019 (Fig. 2a and Fig. S3). The cold surge strengthened the northeasterly winds near the surface and the regional topography channeled the flow toward the equator, resulting in cross-equatorial northwesterly flow or CENS at 0800 UTC (Figs. 2a, c-f). At 0900 UTC, the strong cross-equatorial flow infiltrated the northwestern coast of Java (Fig. 2b) and transported an amount of water vapor to Jakarta. This led to heavy precipitation over the region, consistent with the first peak of precipitation at around 1000 UTC (Figs. 2g-h).

As the CENS persisted (Figs. 2a,b), the strong northwesterly winds continued to cross the equator for at least 12 hours, so that the intrusion of water vapor over Jakarta continued intensively after 1000 UTC (Figs. 2 b,e and Figs. 2 i,j). As a result, a massive amount of water vapor was transported by the strong northwesterly winds, leading to more intense precipitation during this period. This is consistent with the second highest precipitation's peak at 2100 UTC on December 31, 2019 (Fig. 1b). From 2300 UTC onward, the CENS began to dissipate (Fig. 2a) and caused a decrease in water vapor transport into the region and hence, reduced precipitation (Fig. 1b). The strong CENS-induced moisture transport during this period is consistent with a large pressure gradient at sea level and surface temperature gradient between the South China Sea and the north Java Sea (Fig. S4).

The intense moisture transport in the presence of the CENS is also confirmed by the backward trajectory of moisture analysis based on the HYSPLIT model (Figs. 2k-l). It is evident that moisture was transported to Jakarta mainly through one route from the South China Sea migrating to the north coast of Java (Fig. 2k). This is also consistent with the transport pathways of IVT during the period of the CENS (color shading). Overall, in the presence of the CENS the South China Sea contributed most of the moisture (59.81%), followed by the southern part of Sumatra Island (26.81%). We also notice a relatively small (2.76%) contribution of moisture source from the Southern Indian Ocean, which might contribute to the local increase in moisture over Jakarta. To summarize, a strong and persistent CENS prior to and during the extreme precipitation event in early January 2020 played a major role in increasing moisture transport towards Jakarta, leading to deep convection and heavy rainfall over the region.

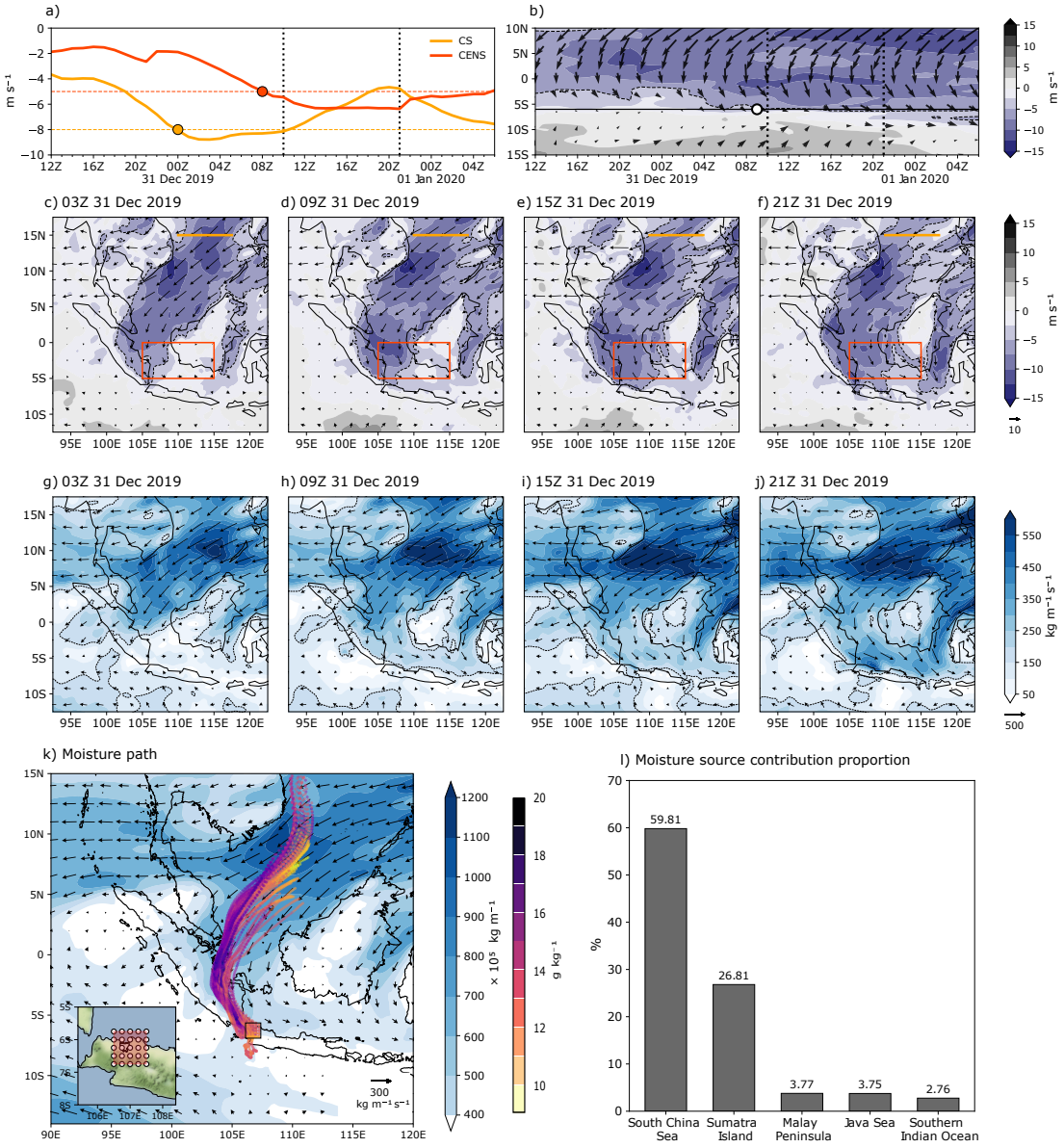

Figure 2. (a) Hourly evolution of CS and CENS indices from 1200 UTC 31 Dec 2019 to 0600 UTC 1 Jan 2020. The red (orange) circle indicates the period when CENS (CS) is active (i.e., exceeding 5 m s^{-1} for CENS (red line) and 8 m s^{-1} for CS (orange line)). The two vertical lines indicate the first and second peaks of the observed precipitation (i.e., at 10Z and 21Z, respectively). (b) Time-latitude cross-sections of the meridional wind component at 925 hPa (shading) and the wind vectors averaged over 106.62° and 107.04°E. The white circle indicates the period when CENS finally intruded into the northern coastline of Java Island (∼0900 UTC). (c-f) Time evolution of meridional wind component (shading) and horizontal wind vectors (m/s) at 925 hPa from 0400 UTC 30 Dec 2019 to 2200 UTC 31 Dec 2019. The red (orange) rectangular box (line) is the area used for defining CENS (CS). (g-j) As in (c-f) but for the evolution of column integrated water vapor transport (IVT) (shading, kg $m^{-1}s^{-1}$) and the corresponding fluxes (vectors). (k) The 72-h backward trajectories of the moisture responsible for the extreme precipitation event. Blue shading indicates the time-integrated IVT for 72-h prior to the period of maximum precipitation (2100 UTC). (l) The relative moisture contributions from the different source regions (see Section 3.2. and text S2 for details).

5.2 The role of equatorial waves and MJO

In addition to the CENS, the effects of concurrent occurrences of convectively active phases of multiple large-scale equatorial waves and MJO also contributed to the development of extreme rainfall in Jakarta (Figure 3). It is evident that since December 31, 2019, three types of equatorial wave modes, including Kelvin waves, TD-type waves, and EIG waves had occurred concurrently with a convective phase of MJO. These concurrent occurrences resulted in significant negative OLR anomalies (enhanced large-scale convection) over Jakarta (Fig. 3a).

More specifically, the convectively active phase of Kelvin waves were observed over Jakarta on 31 December 2019 and lasted for a few days (Figs. 3a, c), while the TD-type waves and EIG waves emerged a few days before the end of 2019 and continued until early January 2020 (Figs. 3a,e,f). Unlike these three types of equatorial waves, the MRG wave was in its dry phase during the period of extreme rainfall (Fig. 3g) and ER wave activity had not yet reached Jakarta. Therefore, the MRG and ER waves did not contribute to the anomalous convective activity during the event (Figs. 3a,d,g). The convective phase of MJO over Jakarta, on the other hand, had occurred since 27 December 2019, and lasted until 3 January 2020, as it moved slowly eastward and then transitioned to the dry phase (Fig. 3a, b). The existence of the MJO above the Maritime Continent is confirmed by other global MJO indices calculated based on univariate EOF analysis of OLR (Figs. S6a-c), in which the MJO was in its transition phases from 4 to 5, with a relatively weak amplitude. However, its activity over the Maritime Continent was not observed in the multivariate MJO indices, such as VPM and RMII (i.e. MJO was in weak phase 8, see Figs. S6d-e). This is because the global multivariate MJO indices tend to be more associated with the wind circulation than the convection, while the filtered OLR is much more tied to the convection (cf. Straub (2013); Gottschalck et al. (2013)).

The contribution of each wave mode to the anomalous precipitation during the period of extreme event is summarized in Fig. 3h. Of the total anomalous precipitation (110 mm/day) on 31 December 2019 observed from NASA IMERG, about ∼23% can be attributed to equatorial waves and MJO (see also Fig. S5b for the total precipitation modulated by these waves and MJO). The Kelvin, TD-type, and EIG waves made a strong positive contribution to the rainfall anomaly (∼20%), while MJO only asserted a weak positive influence (∼3%). The positive contribution of these wave modes and MJO to the total anomaly are consistent with the increase in low-level convergence of moisture flux induced by their activities, leading to an enhancement of local convection and hence, increased precipitation over the region (Fig. 3h).

Finally, it is important to note that even though the convective center associated with the ER waves had not reached Jakarta during the event (Fig. 3a), the large-scale circulation induced by these waves played a significant role in modulating the cross-equatorial transport of moisture toward Jakarta (Fig. S7). Our results indicate that the anomalous meridional flow was largely attributed to ER waves (Fig. S7). Therefore, it can be inferred that the indirect effect of ER waves was to enhance the southerly flow from the South China Sea toward the Java Sea, leading to the increased moisture transport induced by CENS. In summary, Kelvin waves, TD-type waves, EIG waves and MJO significantly contributed to the extreme precipitation event in Jakarta.

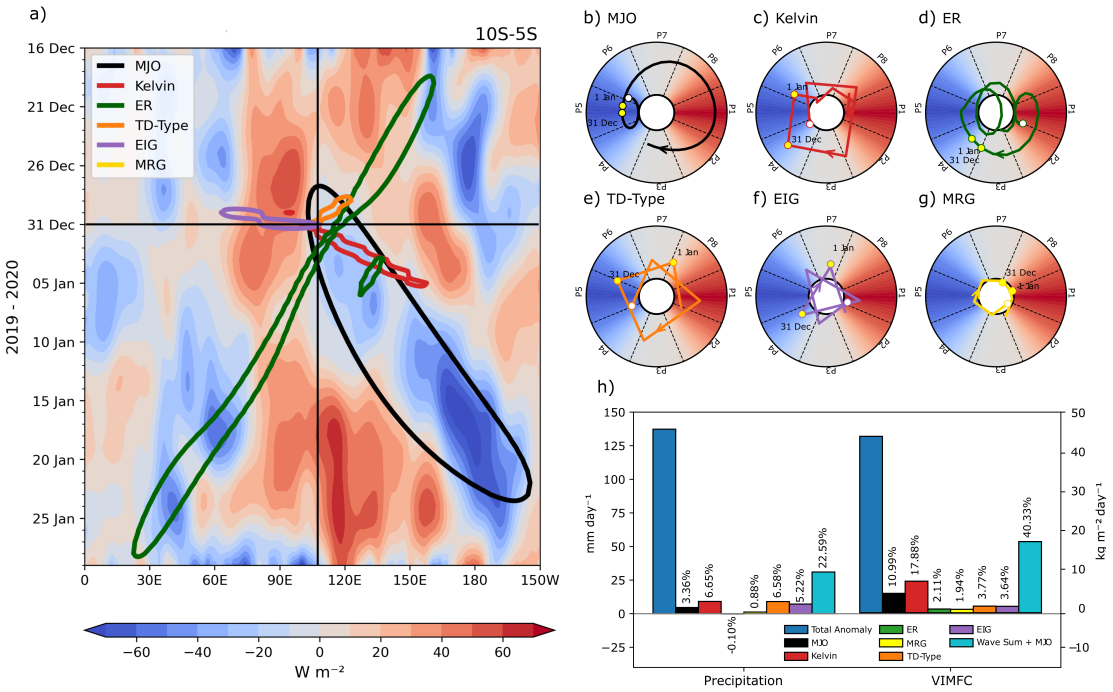

Figure 3. (a) Time-longitude section of OLR anomalies averaged over 10°S-5°S, with an interval of 10 Wm^{-2} (color shading). Contour lines show the amplitudes of selected equatorial modes and MJO that have been wavenumber-frequency-filtered (see details in Section 3.3 and Table S1). The contour line for MJO is -17.12 W/m (-2 stddev), for Kelvin waves: -13.48 W/m (-2 σ), for ER waves: -17.58 W/m (-2σ), for TD-Type waves: -7.56 W/m (-1.5σ) and for EIG waves: -5.45 W/m (-1.5σ), where σ is the standard deviation. The vertical line at 107°E marks the location of the city of Jakarta. The horizontal line depicts the period of 31 December 2019. Only the wet phases of the equatorial waves and MJO that occur during the major flood event are shown. (b-g) Local wave phase diagrams of MJO and different types of equatorial waves during the major flood event. The two yellow dots indicate the period of 31 December 2019 and 1 January 2020. The local wave phase diagrams are constructed from the standardized wave-filtered OLR and its tendency centered at 106.5°E (reference longitude). Phases 4-6 (1-2 and 8) are termed as wet (dry) phases throughout the life cycle of waves. (h) Contribution of different types of equatorial waves and MJO on the total daily precipitation and VIMFC anomalies during the Jakarta Flood in 31 January 2019. The percentage (%) is calculated as a ratio of the each filtered-wave anomaly and the total anomaly (blue bar).

5.3 Mesoscale Convective System

The occurrence of extreme rainfall and the corresponding flooding event is often associated with the mesoscale convective system (MCS), which are more favorable in the presence of CENS, equatorial waves, and MJO (Wu et al., 2007; Mapes et al., 2006; Schumacher & Johnson, 2008; Latos et al., 2021). Here, we would like to understand the characteristics of the MCS over Jakarta in the presence of those forcing during the period of the extreme rainfall events.

Figure 4 shows the time evolution of the MCS superimposed with the total precipitation estimated by radar. The MCS over the land began to develop at 0500 UTC on 31 December 2019 from around 7°S (Fig. 4a), over the mountains to the south of Jakarta.

At 0600 UTC, the MCS grew stronger and moved northward toward Jakarta (Figs. 4b,c). This development and its northward propagation was very likely driven by the near-surface convergence due to the interaction of cloud outflow and warm-moist air near the surface (Wu et al., 2007; Mori et al., 2018). At around 0900 UTC, the MCS became more mature and reached Jakarta (Fig. 4d). As the CENS started around 0800 UTC and reached the coast of Java island at around 0900 UTC (Fig. 2a), the maturation stage of the MCS during this period was associated with the enhanced moisture induced by the CENS over the region, which resulted in a stronger updraft and deeper convection (see convective index development in the presence of CENS in Fig. S8 in Supporting Information). Consistent with the development of the MCS during this time, the first peak of precipitation was observed over Jakarta at around 1000 UTC.

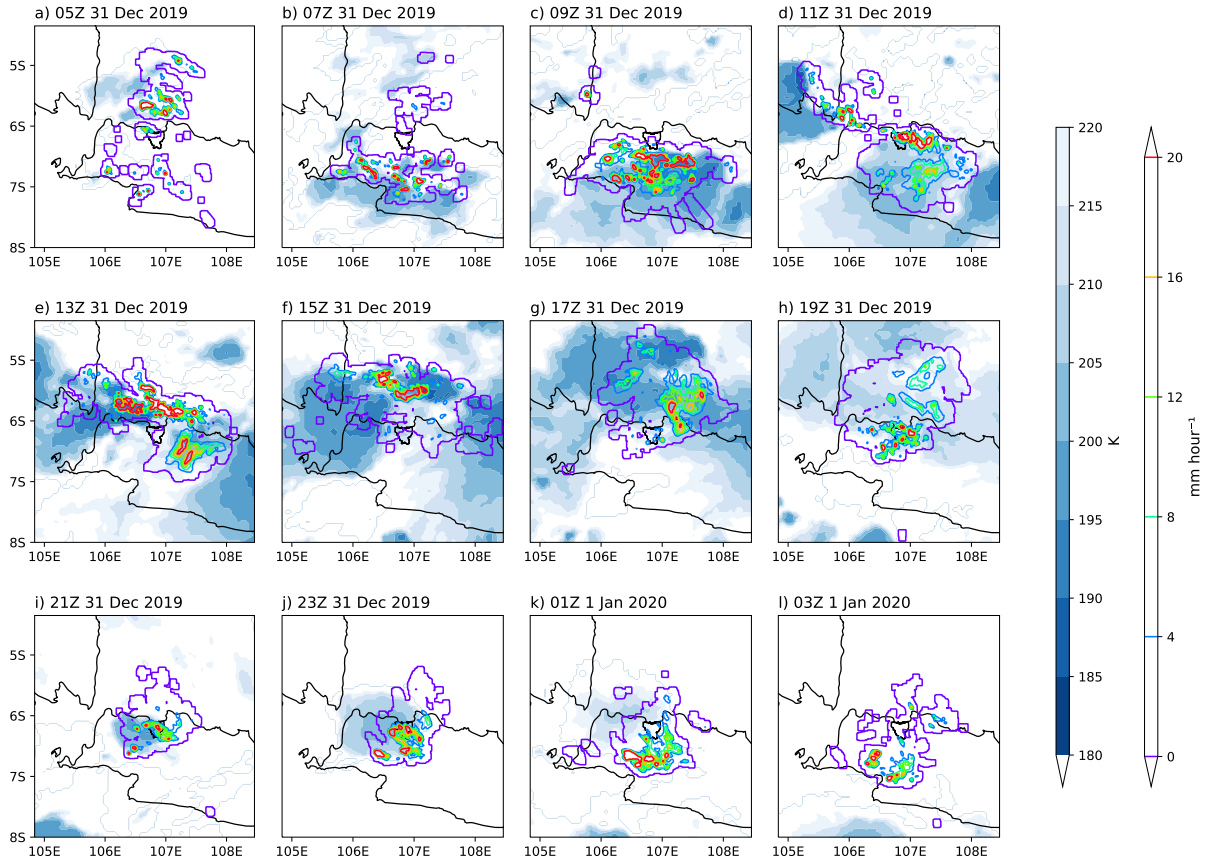

Figure 4. Time evolution of the mesoscale convective system (MCS) calculated based on temperature black body (TBB) retrieved from Himawari satellite (color shading) superimposed with total precipitation (mm) estimated by a C-band Doppler radar (contour lines) from 0500 UTC 31 December 2019 to 0300 UTC 1 January 2020. The color gradation from light to dark blue indicates interior cold cloud with TBB $\leq$ 221 K.

The MCS continued to migrate northward after 1000 UTC, reaching the Java Sea at 1300 UTC (Figs. 4e,f). The MCS grew stronger at 1700 UTC over the Java sea and started to dissipate at 1900 UTC (Fig. 4h). At 2100 UTC, MCS started to grow locally over the region of Jakarta (onshore) until 2300 UTC (Fig. 2j). This MCS growth could have been due to the intrusion of the northerly wind into the MCS during the active phase of CENS (Fig. 2a) and the near-surface convergence lines from the interaction between

the cloud outflow and the northerly wind (Wu et al., 2007; Mori et al., 2018). In this case, CENS acted as an inflow to the preceding MCS, causing it to grow (Mori et al., 2018). This is consistent with strong and persistent CENS-induced moisture transport and convective activity during this period (Fig. 2a and Fig. S8). At this stage, the MCS brought rainfall over Jakarta, marking the second peak of the extreme rainfall at around 2100-2200 UTC. Thereafter, the MCS propagated southward and dissipate at 0300 UTC.

To sum up the heavy rainfall over Jakarta in early January 2020 is associated with MCS. The development of the MCS was closely related to the CENS induced enhanced northerly wind and moisture transport, which promoted vigorous deep convective system over the region. In addition, the convective environment induced by equatorial waves and MJO (Fig. 3 and Fig. S5), which were present prior to and during the extreme event, may also potentially support the development of MCS over Jakarta (e.g., Mapes et al. (2006)). Together, the combined effects of these large-scale forcing factors provided favorable conditions for the development of MCSs, and hence extreme rainfall over Jakarta.

6 Conclusion and Discussion

In this study, we have investigated the large-scale atmospheric driving mechanisms of the torrential rainfall over Jakarta in early January 2020. This extreme event has been unprecedented in the historical rainfall database in Jakarta since 1866, with a return period of 300 years. Our analysis shows that the torrential rainfall event was linked to the large-scale atmospheric circulation and moisture transport/modulation induced by the CENS, equatorial waves, and MJO. The key results of our finding can be summarized as follows:

1. The extreme precipitation event in Jakarta in early January 2020 was mainly caused by an active CENS that occured concurrently with active phases of equatorial waves (mainly Kelvin, TD-type, and EIG waves) and MJO.
2. The strong and persistent lower-level northerly wind and moisture transport induced by the CENS created favorable atmospheric conditions for the development of deep convection and heavy rainfall over Jakarta.
3. Increasing in low-level moisture convergence induced by the three types of equatorial waves and MJO further supported the development of the heavy rainfall over the region, by contributing up to ∼23% to the enhanced local precipitation. On the other hand, the ER waves contributed indirectly to the enhanced northerly moisture transport toward Jakarta by strengthening the cross-equatorial meridional flow.
4. These large-scale dynamical forcing factors together provided a conducive convective environment for the development of MCSs and hence, extreme rainfall over the region.

Our Lagrangian analysis of moisture sources and pathways confirms that the local increase in moisture over Jakarta prior to and during the extreme event was mainly due to the circulation and transport of moisture associated with the CENS. This is consistent with previous studies, showing that CENS-induced strong low-level vertical wind shear and moisture allows severe convection to occur over Jakarta (Wu et al., 2007; Mori et al., 2018). It is also interesting to note that diurnal land convection influences the Maritime Continent response to CENS, leading to the enhanced precipitation over the large islands (Qian, 2008; Mori et al., 2018). Understanding the interaction between the CENS and thermally induced diurnal changes in the boundary-layer wind over Jakarta, leading to enhanced localized convection, requires sensitivity simulations with a high-resolution general circulation model. This will be the subject of future research.

It is noteworthy that although the convectively active phases of Kelvin waves, TD-type waves, EIG waves, and MJO only played a secondary role in the extreme precip-

itation in Jakarta in early 2020, the low-level moisture convergence induced by these waves and MJO significantly contributed to the enhanced local precipitation. This supports the findings of recent studies showing the importance of MJO and equatorial waves in triggering extreme rainfall and flooding events over the Maritime Continent (Baranowski et al., 2020; Ferrett et al., 2020; Lubis & Respati, 2021; Muhammad et al., 2021; Latos et al., 2021; Schreck, 2021).

In a warmer future climate, models project there will be an increased risk of more intense, more frequent, and longer-lasting extreme precipitation (Robinson et al., 2021). Improved understanding of the dynamical mechanisms responsible for such events may provide some insight into this problem under the warmer climates. In addition, the development of novel methodologies for accurate weather predictions could also be achieved through an improved understanding of the underlying dynamics. These results could, therefore, be potentially leveraged to improve predictions of extreme weather-driven hazards in Jakarta in the future.

7 Data Availability Statement

All data used in this manuscript are publicly available. The ERA-5 reanalysis and SST datasets are publicly available at `https://www.ecmwf.int/en/forecasts/datasets/reanalysis-datasets/era5` and `https://psl.noaa.gov/data/gridded/data.ncep.reanalysis2.html`. The NASA GPM data may be obtained from `https://doi.org/10.5067/GPM/IMERGDF/DAY/06`. Other data including in-situ hourly rainfall, radar reflectivity, blackbody temperature of clouds from Himawari-8 satellite, bandpass filtered data, and HYSPLIT backward trajectory data are available at `https://doi.org/10.5281/zenodo.6568356`. Daily global MJO indices are available at `https://psl.noaa.gov/mjo/mjoindex/`.

References

Aldrian, E. (2008). Dominant factors of jakartas three largest floods. *Jurnal Hidrosfir Indonesia*, *3*(3).

Baranowski, D. B., Flatau, M. K., Flatau, P. J., Karnawati, D., Barabasz, K., Labuz, M., ... Marzuki (2020, May 19). Social-media and newspaper reports reveal large-scale meteorological drivers of floods on sumatra. *Nature Communications*, *11*(1), 2503. doi: 10.1038/s41467-020-16171-2

Berlinger, J., & Yee, I. (2020). 66 people now killed by flooding in jakarta, and more rain appears to be on the way. *CNN*. Retrieved 2020-01-06, from `https://edition.cnn.com/2020/01/06/asia/jakarta-floods-intl-hnk/index.html`

Bessho, K., Date, K., Hayashi, M., Ikeda, A., Imai, T., Inoue, H., ... Yoshida, R. (2016). An introduction to himawari-8/9- japan's new-generation geostationary meteorological satellites. *Journal of the Meteorological Society of Japan. Ser. II*, *94*(2), 151-183. doi: 10.2151/jmsj.2016-009

Ferrett, S., Yang, G.-Y., Woolnough, S. J., Methven, J., Hodges, K., & Holloway, C. E. (2020). Linking extreme precipitation in southeast asia to equatorial waves. *Quarterly Journal of the Royal Meteorological Society*, *146*(727), 665-684. doi: https://doi.org/10.1002/qj.3699

Gottschalck, J., Roundy, P. E., III, C. J. S., Vintzileos, A., & Zhang, C. (2013). Large-scale atmospheric and oceanic conditions during the 201112 dynamo field campaign. *Monthly Weather Review*, *141*(12), 4173 - 4196. doi: 10.1175/MWR-D-13-00022.1

Hattori, M., Mori, S., & Matsutomo, J. (2011). The cross-equatorial northerly surge over the maritime continent and its relationship to precipitation patterns. *Journal of the Meteorological Society of Japan. Ser. II*, *89A*, 27-47. doi:

10.2151/jmsj.2011-A02

Heistermann, M., Jacobi, S., & Pfaff, T. (2013). An open source library for processing weather radar data (wradlib). *Hydrology and Earth System Sciences*, *17*(2), 863–871.

Hersbach, H., Bell, B., Berrisford, P., Hirahara, S., Horányi, A., Muñoz-Sabater, J., ... others (2020). The era5 global reanalysis. *Quarterly Journal of the Royal Meteorological Society*, *146*(730), 1999–2049.

Huffman, G. J., Bolvin, D. T., Braithwaite, D., Hsu, K.-L., Joyce, R. J., Kidd, C., ... others (2020). Integrated multi-satellite retrievals for the global precipitation measurement (gpm) mission (imerg). In *Satellite precipitation measurement* (pp. 343–353). Springer.

Kiladis, G. N., Wheeler, M. C., Haertel, P. T., Straub, K. H., & Roundy, P. E. (2009). Convectively coupled equatorial waves. *Reviews of Geophysics*, *47*(2). doi: https://doi.org/10.1029/2008RG000266

Krämer, S., & Verworn, H.-R. (2009). Improved radar data processing algorithms for quantitative rainfall estimation in real time. *Water science and technology*, *60*(1), 175–184.

Latos, B., Lefort, T., Flatau, M. K., Flatau, P. J., Permana, D. S., Baranowski, D. B., ... others (2021). Equatorial waves triggering extreme rainfall and floods in southwest sulawesi, indonesia. *Monthly Weather Review*, *149*(5), 1381–1401.

Liebmann, B., & Smith, C. A. (1996). Description of a complete (interpolated) outgoing longwave radiation dataset. *Bulletin of the American Meteorological Society*, *77*(6), 1275–1277.

Lubis, S. W., & Jacobi, C. (2015). The modulating influence of convectively coupled equatorial waves (ccews) on the variability of tropical precipitation. *International Journal of Climatology*, *35*(7), 1465-1483. Retrieved from `https://rmets.onlinelibrary.wiley.com/doi/abs/10.1002/joc.4069` doi: https://doi.org/10.1002/joc.4069

Lubis, S. W., & Respati, M. R. (2021). Impacts of convectively coupled equatorial waves on rainfall extremes in java, indonesia. *International Journal of Climatology*, *41*(4), 2418–2440.

Mapes, B., Tulich, S., Lin, J., & Zuidema, P. (2006). The mesoscale convection life cycle: Building block or prototype for large-scale tropical waves? *Dynamics of Atmospheres and Oceans*, *42*(1), 3-29.

Marshall, J., Langille, R., & Palmer, W. M. K. (1947). Measurement of rainfall by radar. *Journal of Atmospheric Sciences*, *4*(6), 186–192.

Mori, S., Hamada, J.-I., Hattori, M., Wu, P.-M., Katsumata, M., Endo, N., ... Yamanaka, M. D. (2018, Sep 03). Meridional march of diurnal rainfall over jakarta, indonesia, observed with a c-band doppler radar: an overview of the harimau2010 campaign. *Progress in Earth and Planetary Science*, *5*(1), 47. doi: 10.1186/s40645-018-0202-9

Muhammad, F. R., Lubis, S. W., & Setiawan, S. (2021). The influence of boreal summer madden-julian oscillation on precipitation extremes in indonesia. *arXiv preprint arXiv:2112.00001*.

Nie, Y., & Sun, J. (2022). Moisture sources and transport for extreme precipitation over henan in july 2021. *Geophysical Research Letters*, *49*(4), e2021GL097446. doi: https://doi.org/10.1029/2021GL097446

Nisa, K. (2020). Rekapitulasi data banjir dki jakarta dan penanggulangannya tahun 2020. *Statistik DKI Jakarta*. Retrieved 2020-01-15, from `https://statistik.jakarta.go.id/rekapitulasi-data-banjir-dki-jakarta-dan-penanggulangannya-tahun-2020/`

Nuryanto, D. E., Pawitan, H., Hidayat, R., & Aldrian, E. (2019). Characteristics of two mesoscale convective systems (mcss) over the greater jakarta: case of heavy rainfall period 15–18 january 2013. *Geoscience Letters*, *6*(1), 1–15.

Nuryanto, D. E., Pawitan, H., Hidayat, R., & Aldrian, E. (2021). The occurrence of the typical mesoscale convective system with a flood-producing storm in the wet season over the greater jakarta area. *Dynamics of Atmospheres and Oceans*, *96*, 101246. doi: https://doi.org/10.1016/j.dynatmoce.2021.101246

Paski, J. A., Alfahmi, F., Permana, D. S., & Makmur, E. E. (2020). Reconstruction of extreme rainfall event on september 19-20, 2017, using a weather radar in bengkulu of sumatra island. *The Scientific World Journal*, *2020*.

Peatman, S. C., Schwendike, J., Birch, C. E., Marsham, J. H., Matthews, A. J., & Yang, G.-Y. (2021). A local-to-large scale view of maritime continent rainfall: control by enso, mjo and equatorial waves. *Journal of Climate*, 1 - 52. Retrieved from `https://journals.ametsoc.org/view/journals/clim/aop/JCLI-D-21-0263.1/JCLI-D-21-0263.1.xml` doi: 10.1175/JCLI-D-21-0263.1

Qian, J.-H. (2008). Why precipitation is mostly concentrated over islands in the maritime continent. *Journal of the Atmospheric Sciences*, *65*(4), 1428 - 1441. doi: 10.1175/2007JAS2422.1

Ramadhan, R., Marzuki, M., Yusnaini, H., Muharsyah, R., Suryanto, W., Sholihun, S., ... Hashiguchi, H. (2022). Capability of gpm imerg products for extreme precipitation analysis over the indonesian maritime continent. *Remote Sensing*, *14*(2). Retrieved from `https://www.mdpi.com/2072-4292/14/2/412` doi: 10.3390/rs14020412

Reynolds, R. W., Rayner, N. A., Smith, T. M., Stokes, D. C., & Wang, W. (2002). An improved in situ and satellite sst analysis for climate. *Journal of Climate*, *15*(13), 1609 - 1625. doi: 10.1175/1520-0442(2002)015⟨1609:AIISAS⟩2.0.CO;2

Riley, E. M., Mapes, B. E., & Tulich, S. N. (2011). Clouds associated with the madden julian oscillation: A new perspective from cloudsat. *Journal of the Atmospheric Sciences*, *68*(12), 3032 - 3051. doi: 10.1175/JAS-D-11-030.1

Robinson, A., Lehmann, J., Barriopedro, D., Rahmstorf, S., & Coumou, D. (2021, Oct 05). Increasing heat and rainfall extremes now far outside the historical climate. *npj Climate and Atmospheric Science*, *4*(1), 45. doi: 10.1038/s41612-021-00202-w

Sakaeda, N., Kiladis, G., & Dias, J. (2020). The diurnal cycle of rainfall and the convectively coupled equatorial waves over the maritime continent. *Journal of Climate*, *33*(8), 3307 - 3331. doi: 10.1175/JCLI-D-19-0043.1

Schreck, C. J. (2021). Global survey of the mjo and extreme precipitation. *Geophysical Research Letters*, *48*(19), e2021GL094691. Retrieved from `https://agupubs.onlinelibrary.wiley.com/doi/abs/10.1029/2021GL094691` doi: https://doi.org/10.1029/2021GL094691

Schumacher, R. S., & Johnson, R. H. (2008). Mesoscale processes contributing to extreme rainfall in a midlatitude warm-season flash flood. *Monthly Weather Review*, *136*(10), 3964 - 3986. doi: 10.1175/2008MWR2471.1

Siswanto, Van Oldenborgh, G. J., Van Der Schrier, G., Lenderink, G., & Van Den Hurk, B. (2015). 26. trends in high-daily precipitation events in jakarta and the flooding of january 2014. *Bulletin of the American Meteorological Society*, *96*(12), S131–S135.

Stein, A., Draxler, R. R., Rolph, G. D., Stunder, B. J., Cohen, M., & Ngan, F. (2015). Noaas hysplit atmospheric transport and dispersion modeling system. *Bulletin of the American Meteorological Society*, *96*(12), 2059–2077.

Straub, K. H. (2013). Mjo initiation in the real-time multivariate mjo index. *Journal of Climate*, *26*(4), 1130 - 1151. doi: 10.1175/JCLI-D-12-00074.1

Trilaksono, N. J., Otsuka, S., Yoden, S., Saito, K., & Hayashi, S. (2011). Dependence of model-simulated heavy rainfall on the horizontal resolution during the jakarta flood event in january-february 2007. *Sola*, *7*, 193–196.

Wheeler, M., & Kiladis, G. N. (1999). Convectively coupled equatorial waves: Analysis of clouds and temperature in the wavenumberfrequency domain. *Journal of the Atmospheric Sciences*, *56*(3). doi: 10.1175/1520-0469(1999)056⟨0374:

CCEWAO⟩2.0.CO;2

Whitehall, K., Mattmann, C. A., Jenkins, G., Rwebangira, M., Demoz, B., Waliser, D., ... others (2015). Exploring a graph theory based algorithm for automated identification and characterization of large mesoscale convective systems in satellite datasets. *Earth Science Informatics*, *8*(3), 663–675.

Wu, P., Arbain, A. A., Mori, S., Hamada, J.-i., Hattori, M., Syamsudin, F., & Yamanaka, M. D. (2013). The effects of an active phase of the madden-julian oscillation on the extreme precipitation event over western java island in january 2013. *Sola*, *9*, 79–83.

Wu, P., Hara, M., Fudeyasu, H., Yamanaka, M. D., Matsumoto, J., Syamsudin, F., ... Djajadihardja, Y. S. (2007). The impact of trans-equatorial monsoon flow on the formation of repeated torrential rains over java island. *Sola*, *3*, 93–96.

Supporting Information for "Record-Breaking Precipitation in Indonesia's Capital Jakarta in January 2020 Linked to the Northerly Surge, Equatorial Waves, and MJO"

Sandro W. Lubis[1] *, Samson Hagos [1], Eddy Hermawan [2], Muhamad R. Respati [3], Ainur Ridho [4], Risyanto [2], Fadhlil R. Muhammad [5], Jaka A. I. Paski [6], Siswanto [6], Dian Nur Ratri [6,7], Sonny Setiawan [8], Donaldi S. Permana [6]

[1]Pacific Northwest National Laboratory, Richland, Washington, USA

[2]National Research and Innovation Agency (BRIN), Indonesia

[3]School of Earth, Atmosphere and Environment, Monash University, Australia

[4]Search Engine for Risk and Actions on Resilience, Indonesia

[5]School of Earth Sciences, University of Melbourne, Australia

[6]Indonesia Agency for Meteorology Climatology and Geophysics, Indonesia

[7]Wageningen University and Research, Netherlands

[8]Department of Geophysics and Meteorology, IPB University, Indonesia

*902 Battelle Blvd, Richland, WA 99354, USA

Contents of this file

1. Text S1 to Sx
2. Figures S1 to Sx
3. Tables S1 to Sx

Text S1. Relative moisture source contributions

For calculating the moisture sources proportion, we divided the moisture source area into four land regions and four ocean regions; the demarcation map can be seen in Fig. S1. The method for calculating the moisture source's proportion to the target area is based on a Lagrangian diagnostic, similar to Nie and Sun (2022). We evaluate the moisture changes using the inverse of backward trajectories from an ensemble member trajectory with an initial height of 500 m to 2000 m around Jakarta. A moisture source attribution is identified by the location of increasing change in the specific humidity of a particle or evaporation event during a transport time interval. Decreasing change in the specific humidity during a transport time interval is calculated as a precipitation event. The final moisture source proportion from the source area to the target location is weighted by considering a series of precipitation and evaporation events en route.

Text S2. Local phase diagram

In this method, wave-filtered OLR anomalies are first averaged over 10°S-5°S, corresponding to the location of the observation. The annual cycle is removed before the filtering by subtracting the first three harmonics. The linear trend is then removed from the anomalous fields, and a split-cosine-bell tapering is applied to about 10% of both ends of the time series to minimize the spectral leakage. The latitudinal averaged OLR anomaly and its time derivative are then standardized by dividing them by their respective global standard deviations. These values are then plotted in eight phases, according to their amplitude, the phases 4-6 indicate enhanced regional convection by the equatorial

wave, whereas warm colors (phases 8, 1-2) correspond to suppressed regional convection. This method has been widely used to study the regional influence of equatorial waves on precipitation in many other locations (e.g., van der Linden, Fink, Pinto, Phan-Van, and Kiladis (2016); Schlueter, Fink, Knippertz, and Vogel (2019); Lubis and Respati (2021); Latos et al. (2021)).

Text S3. Water vapor transport and moisture flux convergence

The IVT and VIMFC are calculated from total fields and then filtered with respect to the different frequency-wavenumber (see Table S1). The IVT is calculated using ERA5 zonal and meridional winds and specific humidity as follow:

$$\mathrm{IVT} = \left[\left(\frac{1}{g} \int qu \ \mathrm{d}p \right)^2 + \left(\frac{1}{g} \int qv \ \mathrm{d}p \right)^2 \right]^{1/2} \tag{1}$$

where q is specific humidity, u is zonal wind, and v is meridional wind. The VIMFC is calculated from the moisture budget equation:

$$-\frac{1}{g} \int \left(\frac{\partial q}{\partial t} \right) \ \mathrm{d}p \underbrace{-\frac{1}{g} \int \left(\vec{\nabla} \cdot q\vec{V} \right) \ \mathrm{d}p}_{\mathrm{VIMFC}} - \frac{1}{g} \int \left(\frac{\partial \left(q\omega \right)}{\partial p} \right) \ \mathrm{d}p = P - E \tag{2}$$

where $\vec{V}$ is horizontal wind, ω is vertical velocity, P is precipitation, and E is evaporation. VIMFC is a good measure to equatorial wave and MJO modulation on rainfall as it is directly related to the net precipitation (Lubis & Respati, 2021).

References

Latos, B., Lefort, T., Flatau, M. K., Flatau, P. J., Permana, D. S., Baranowski, D. B., ... others (2021). Equatorial waves triggering extreme rainfall and floods in southwest sulawesi, indonesia. *Monthly Weather Review*, *149*(5), 1381–1401.

Lubis, S. W., & Respati, M. R. (2021). Impacts of convectively coupled equatorial waves on rainfall extremes in java, indonesia. *International Journal of Climatology*, *41*(4), 2418–2440.

Nie, Y., & Sun, J. (2022). Moisture sources and transport for extreme precipitation over henan in july 2021. *Geophysical Research Letters*, *49*(4), e2021GL097446. doi: https://doi.org/10.1029/2021GL097446

Schlueter, A., Fink, A. H., Knippertz, P., & Vogel, P. (2019). A systematic comparison of tropical waves over northern africa. part i: Influence on rainfall. *Journal of Climate*, *32*(5), 1501 - 1523. doi: 10.1175/JCLI-D-18-0173.1

van der Linden, R., Fink, A. H., Pinto, J. G., Phan-Van, T., & Kiladis, G. N. (2016). Modulation of daily rainfall in southern vietnam by the maddenjulian oscillation and convectively coupled equatorial waves. *Journal of Climate*, *29*(16), 5801 - 5820. doi: 10.1175/JCLI-D-15-0911.1

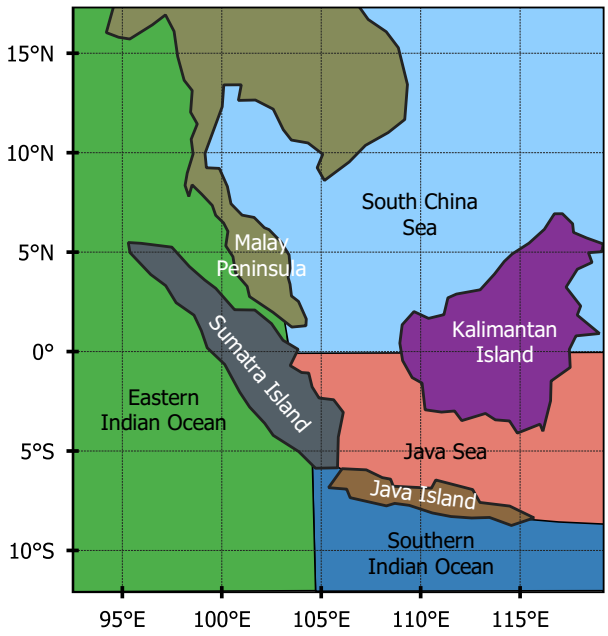

Figure S1. The division of 8 regions, including four land regions and four ocean regions, for the moisture source contribution analysis. The land regions include Sumatra Island, Java Island, Kalimantan Island and the Malay Peninsula. The ocean regions include the the South China Sea, the Java Sea, the eastern Indian Ocean and the southern Indian Ocean.

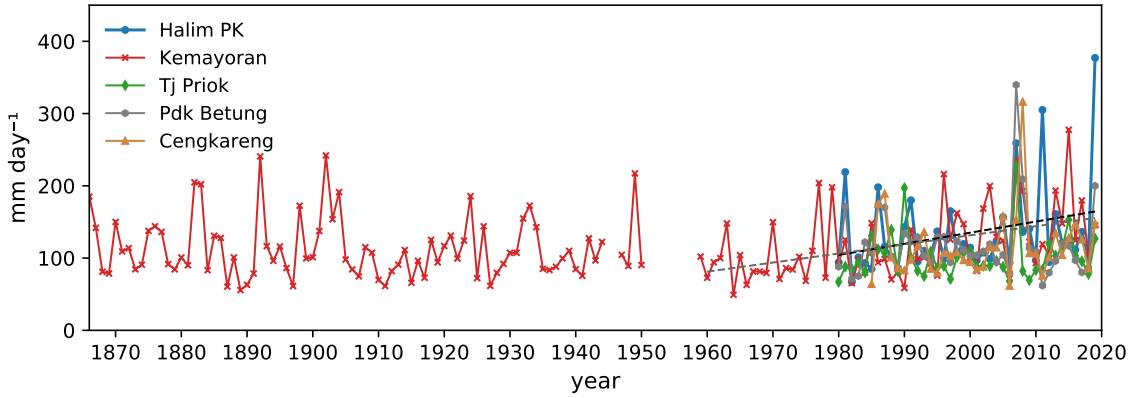

Figure S2. Time series of annual maximum daily precipitation (RX1 day) from 5 rain gauge stations from 1960-1900 (note: only data from Kemayoran station is available back to 1866). The precipitation trend corresponding to the year 1960-2020 (1980-2020) at Kemayoran (Halim) is 12.23 (15.41) mm/decade.

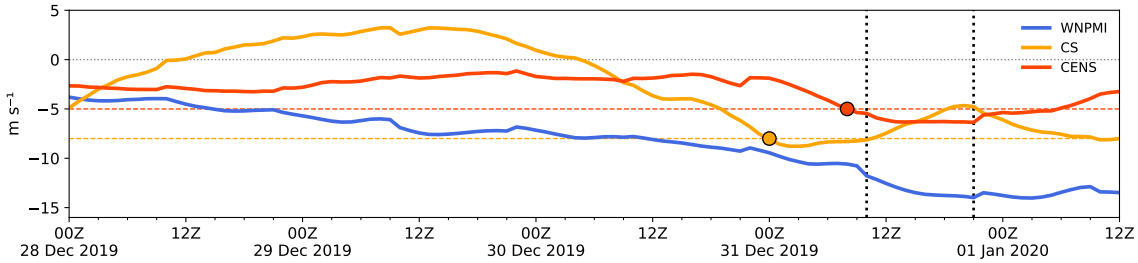

Figure S3. Hourly evolution of cold surge (CS), cross-equatorial northerly surge (CENS), and western North Pacific monsoon index (WNPMI) indices from 0000 UTC 28 December 2019 to 1200 UTC 1 January 2020. The red (orange) circle indicates the period when CENS (CS) is active (i.e., exceeding 5 m s^{-1} for CENS (red line) and 8 m s^{-1} for CS (orange line)). The two vertical lines indicate the first and second peaks of the precipitation (i.e., at 10Z and 22Z, respectively). The WNPMI is defined as the difference of 850-hPa zonal wind between a southern region (5°-15°N, 100°-130°E) and a northern region (20°-30°N, 110°-140°E).

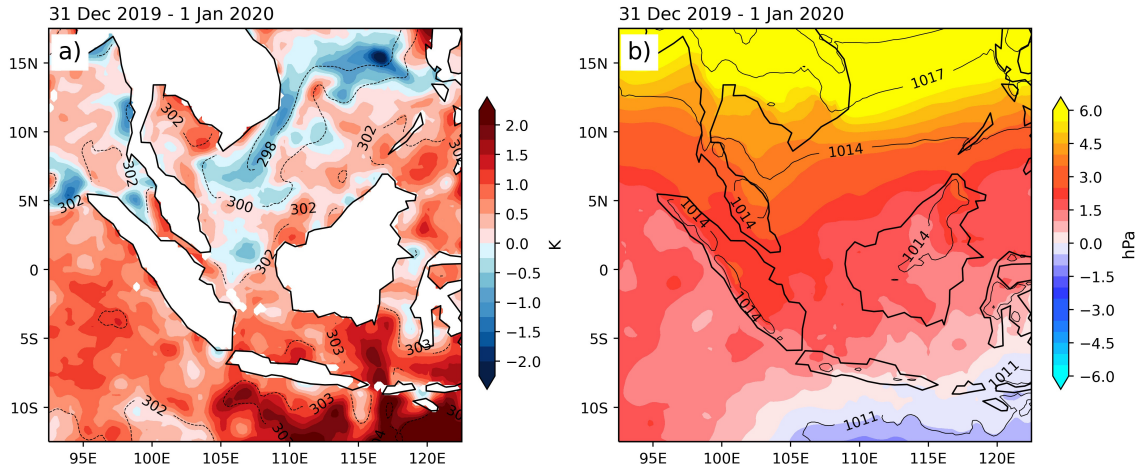

Figure S4. (a) Sea surface temperature (SST) and (b) mean sea-level pressure (MSLP) anomalies averaged from 31 December 2019 to 1 January 2020. Superimposed black contours are the corresponding total field.

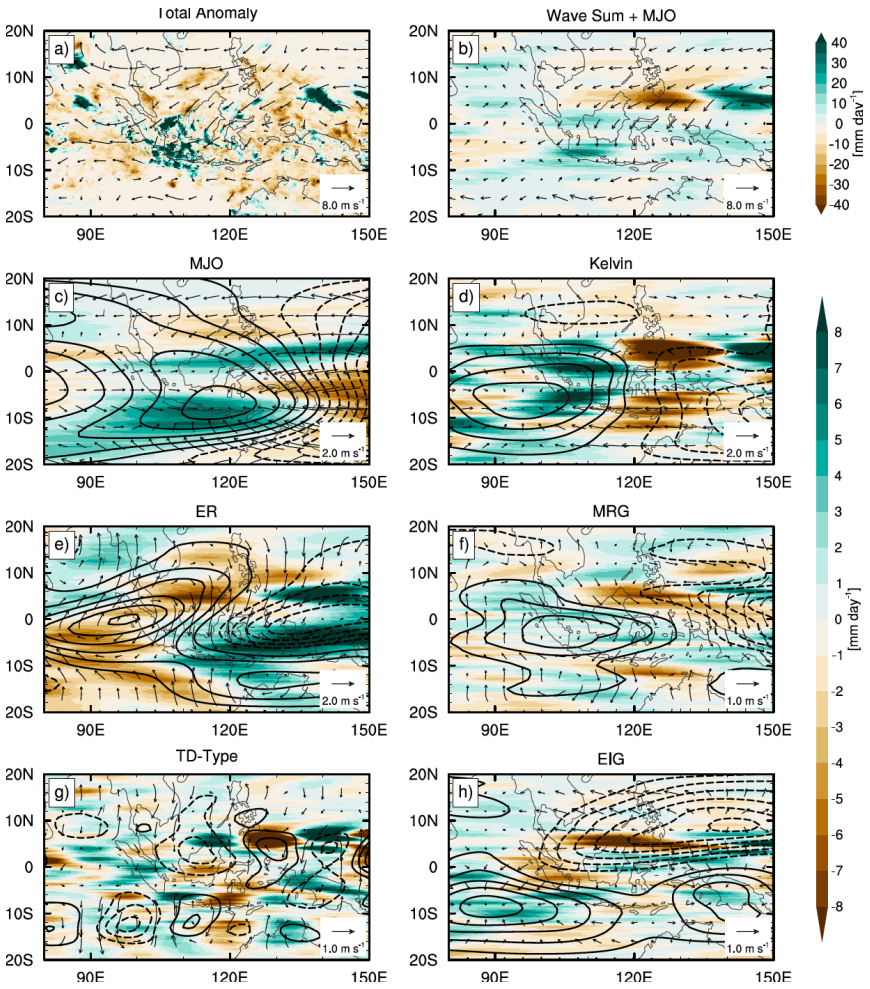

Figure S5. Contribution of different types of CCEWs and MJO on the total daily precipitation anomalies (color shading) during the extreme precipitation event on 31 December 2019. (a) Total anomalies and their corresponding wind vector anomalies, (b) CCEWs- and MJO-filtered anomalies and their corresponding wind vector anomalies, (c) MJO-filtered anomalies and their corresponding divergent wind vectors, (d) Kelvin wave-filtered anomalies and their corresponding divergent wind vectors, (e) ER wave-anomalies and their corresponding rotational wind vectors, (f) MRG wave-filtered anomalies and their corresponding rotational wind vectors, (g) TD-type wave-filtered anomalies and their corresponding rotational wind vectors, and (h) EIG wave filtered anomalies and their corresponding divergent wind vectors. Solid (dashed) contours lines in (e, f, g) indicate positive (negative) values of the stream function anomalies at interval of 5.0 $\times$ 10^6 m^2s^{-1}. Solid (dashed) contours lines in (c, d, h) indicate positive (negative) values of the velocity potential anomalies at an interval of 3.0 $\times$ 10^6 m^2s^{-1}.

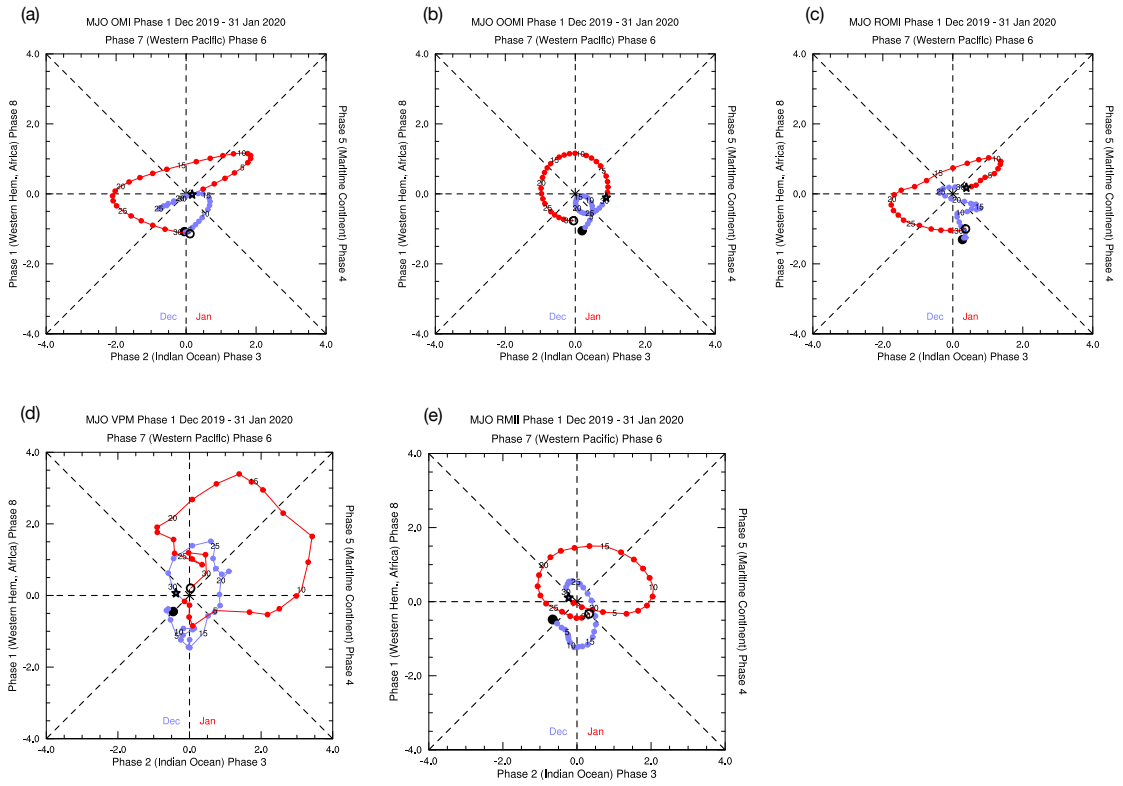

Figure S6. Global MJO indices from 1 December 2019 to 31 January 2020. (a) OLR MJO index (OMI), (b) original OLR MJO Index (OOMI), (c) real-time OLR MJO index (ROMI), (d) velocity potential MJO multivariate index (VPM), and (e) realtime multivariate index for tropical intraseasonal oscillations (RMII). The star indicates the period of the extreme precipitation event on 31 December 2019.

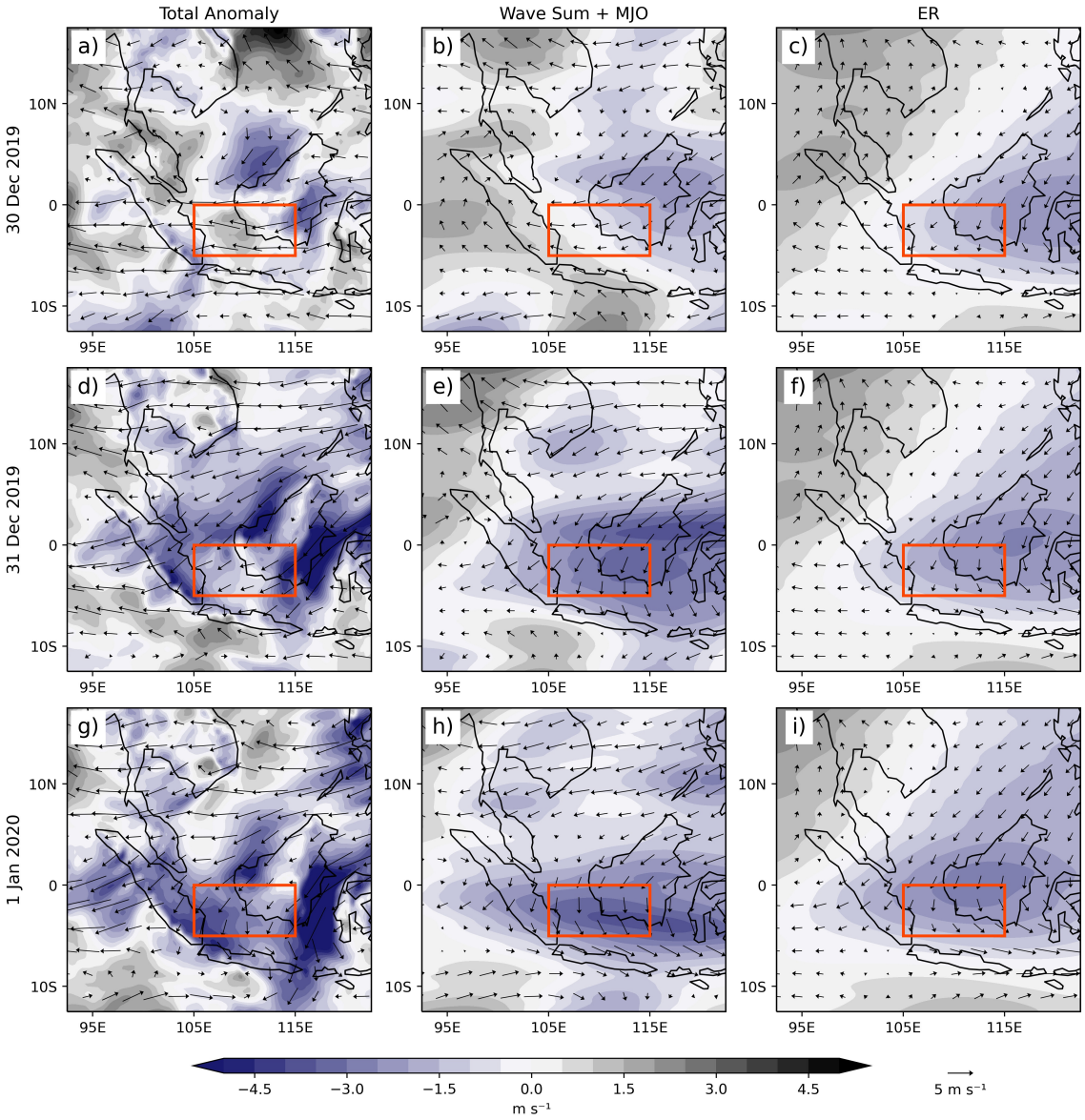

Figure S7. Time evolution of daily mean meridional wind (color shading) and horizontal wind vector anomalies at 925 hPa from 30 December 2019 to 1 January 2020. (a, d, g) Total anomalies, (b, e, h) sum of CCEWs- and MJO-filtered anomalies and (c, f, i) ER wave-filtered anomalies. The red rectangular box indicates the area where CENS is defined.

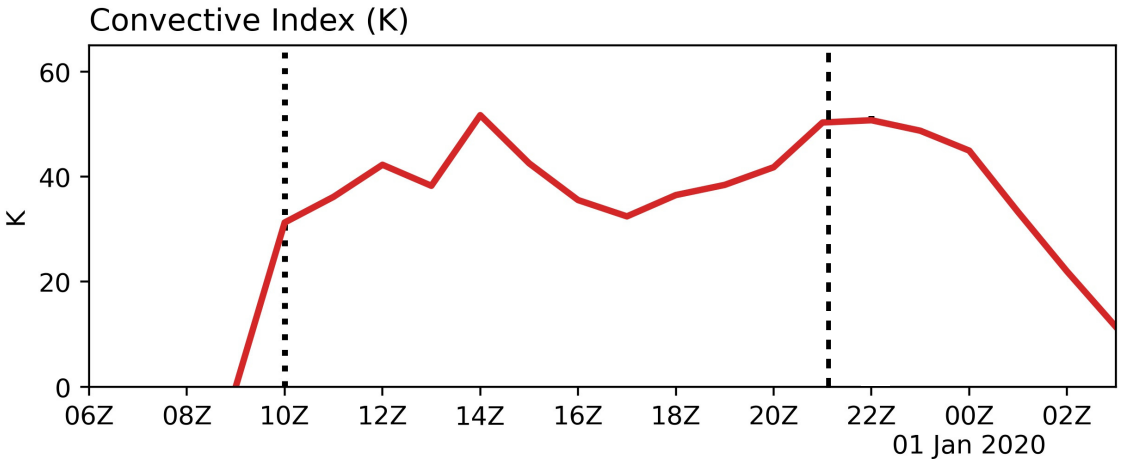

Figure S8. Hourly evolution of convective index (CI) defined by taking temperature below a threshold value of equivalent black body temperature. The threshold value used is 253 K as a measure of convective clouds. CI is averaged over the flood region (regional box in Fig.1a). The two vertical lines indicate the first and second peaks of the observed precipitation (i.e., at 10Z and 21Z, respectively).

Table S1. The period, wavenumber, and equivalent depth used for isolating CCEWs.

Wave Mode	Periods (days)	Wavenumber	Depth (m)
Kelvin	2.5 - 17	1 - 14	8 - 90
Equatorial Rossby (ER)	9 - 72	1 - 10	8 - 90
Mixed Rossby-gravity (MRG)	3 - 10	1 - 10	8 - 90
Eastward Inertio Gravity (EIG) n=0	1 - 5	1 - 14	12 - 50
Tropical-depression (TD)-type	2.5 - 5	6 - 20	-